

Article

Research on a New Plant Fiber Concrete-Light Steel Keel Wall Panel

Yuqi Wu ¹, Yunqiang Wu ^{2,3,*} and Yue Wu ^{2,3}

¹ School of Mechanics and Civil Engineering, China University of Mining and Technology, Beijing 100083, China

² Key Lab of Structures Dynamic Behavior and Control of the Ministry of Education, Harbin Institute of Technology, Harbin 150090, China

³ Key Lab of Smart Prevention and Mitigation of Civil Engineering Disasters of the Ministry of Industry and Information Technology, Harbin Institute of Technology, Harbin 150090, China

* Correspondence: qfmz_wyq@163.com

Abstract: With the growing worldwide attention towards environmental protection, the rational utilization of rice straw (RS) has gradually attracted the attention of scholars. This paper innovatively puts forward a solution for rational utilization of RS. A rice straw fiber concrete (RSFC) with good physical and mechanical properties and a rice straw concrete-light steel keel wall panel (RS-LSWP) with low comprehensive heat transfer coefficient and inconspicuous cold bridge phenomenon was designed. Firstly, the preparation method and process of RSFC is described in detail. Then, the physical and mechanical properties of RSFC, such as strength, apparent density, and thermal conductivity were tested. Finally, the thermal properties of the four new types of cold-formed thin-wall steel panels were analyzed using finite element simulation. The results show that the RSFC with a straw length of 5 mm, mass content of 12%, and modifier content of 1% is the most suitable for RS-LSWP. The standard compressive strength, tensile strength, and thermal conductivity of the RSFC are 2.2 MPa, 0.64 MPa, and 0.0862 W/(m·K), respectively. The wall panels with antitype C keel have a low comprehensive heat transfer coefficient and the best insulation effect. This study innovatively provides a technical method for the rational utilization of RS, promotes the application of RS and other agricultural wastes in building materials and the development of light steel housing.

Keywords: bio-based materials and structures; sustainable structures; plant fiber concrete; light steel keel wall panel; thermal performance



Citation: Wu, Y.; Wu, Y.; Wu, Y. Research on a New Plant Fiber Concrete-Light Steel Keel Wall Panel. *Sustainability* **2023**, *15*, 8109. <https://doi.org/10.3390/su15108109>

Academic Editor: Gianluca Mazzucco

Received: 27 March 2023

Revised: 10 May 2023

Accepted: 12 May 2023

Published: 16 May 2023



Copyright: © 2023 by the authors. Licensee MDPI, Basel, Switzerland. This article is an open access article distributed under the terms and conditions of the Creative Commons Attribution (CC BY) license (<https://creativecommons.org/licenses/by/4.0/>).

1. Introduction

Rice straw (RS) is one of the crop straw, whose annual output can reach billions of tons around the world [1]. Asia, one of the major rice-producing regions, produces about 620 million tons of straw every year [2]. However, only a small part of these straws are properly handled by livestock farming, construction materials, etc., and most of them are still burned directly, which not only wastes resources but also has a bad impact on the ecological environment [3].

Rice straw ash contains a lot of silica [4]. To reasonably solve the problem of RS, some scholars have tried to use straw ash as a building material. In 1983, Mehta used rice RS ash for cement concrete [5]. Josefa et al. characterized the ash from different parts of the RS and showed that the reuse of RS ash in the cement system is promising [6]. Blessen et al. have also confirmed the feasibility of using biomass ash from RS as cement concrete materials [6,7]. Rehman, Abou Sekkina, et al. studied how to increase the content of silica in straw ash [4,8]. Agwa et al. studied the use of rice husk ash in cement and showed that RHA-modified cement exhibits better mechanics and durability. Some scholars have studied the effects of RS ash applied in concrete on the setting time, workability, strength, water absorption, porosity and density of concrete [9–13].

As a straw fiber, RS has the advantages of low thermal conductivity and high sound insulation ability, there are many cases where it is directly used to make houses [14]. Some building materials, such as gypsum board and environmentally friendly brick, are also made by mixing straw with cement-based cementitious materials [15–17]. In addition, some scholars used rice husk, sugarcane bagasse ash (SBA), and other agricultural wastes to develop clay bricks [18]. Rice straw fiber reinforced concrete (RSFRC) developed by mixing RS with Portland cement is one of the ways of rational utilization of RS in recent years. Feraidon Ataie et al. studied the effects of adding rice straw fiber (RSF) on the compressive strength and bending strength of concrete, drying shrinkage rate, and heat of hydration of cement [19]. Chinh Van Nguyen et al. studied the properties of rice straw-reinforced alkali-activated cementitious composites (AACC) and found that RS had a very significant positive effect on the performance of AACC, and that alkali treatment was also an effective method for enhancing the bond between the RS and the matrix [20]. In the study of Liu et al., RS were pretreated with NaOH and grafted with Nano-SiO₂ [4]. The modified rice straw fiber reinforced concrete (RSFRC) prepared by them also promoted the application of plant straw fiber in civil engineering [6]. However, some scholars have proven that the plant fiber in Portland cement's strong alkaline environment (pH > 13) will be decomposed and mineralized, which will cause plant fibers to lose their strengthening effect [21–24]. In addition to Portland cement, Sorel et al. [25] developed a magnesium oxychloride cement (MOC) (pH: 8–9.5) with lower alkalinity suitable for mixing with RS. The cement is composed of light-burned magnesium oxide, magnesium chloride hexahydrate, water, and other proprietary materials [26]. MOC has outstanding advantages such as fire resistance, low cost, high strength, fast curing, high wear resistance, and low thermal conductivity [27]. However, low toughness and poor water resistance limit the application of MOC. To improve the performance of MOC, modified MOC have been prepared using fly ash, phosphoric acid, silica powder, silicone acrylic emulsion, and granite waste. All of these additives can improve the water resistance of MOC [28–31]. Xiao et al. invented the foam lightweight MOC material (MOCL) by adding an appropriate amount of H₂O₂ and MgSO₄ in the process of producing MOC. It is lighter, waterproof, and heat-resistant than traditional MOC materials, but the defects of poor toughness and easy cracking have not been completely solved [32]. Wang et al. combined MOC with straw treated with H₂O₂ foaming to develop straw/magnesium lightweight composite (SMLC). Compared with MOC, the production of SMLCS are more energy-saving and environmentally protected. The compressive strength and bending strength of SMLCS are up to 12.5 MPa and 4.8 Mpa, respectively, and the thermal conductivity is 0.06 W/(m·K). However, the additional amount of RS in SMLCS is not very large, amounting to only 0.9% [32].

Meanwhile, with the development of the social economy, houses in rural areas are changing from traditional brick and concrete structures to light and efficient thermal insulation structures. Therefore, light steel structure has gradually received the attention of researchers. The light steel structure is a low-rise and multi-story building structure with a large number of light insulation materials. It takes cold-formed thin-wall steel, light welding or high-frequency welding steel, and light hot rolled steel as the main stress components [33]. Since the 1950s, with the development of the steel structure industry, the characteristics of different types of light steel wallboards have been studied [34–40]. Light steel keel wall panels are mostly filled with glass fiber, rock wool, foamed concrete and other materials, which make the wall panels have a “hollow feeling”, which seriously limits the popularization and application of cold-formed thin-wall steel structure buildings in China. Glass fiber cotton dust produced by rock wool will also directly enter the respiratory system of residents, causing respiratory tract related diseases. In addition, light steel keel have extremely poor thermal insulation performance, as such, scholars have proposed some measures to improve the

thermal insulation and prevent the cold bridge phenomenon of wall panels at keel position [39,40].

Although previously scholars have proposed a better scheme of straw fiber combination with magnesium oxychloride cement (MOC), there are still some problems, such as the small amount of RS, the complicated processing process of straw, cracks appearing after combination; additionally, they do not consider the case of combining straw concrete with light steel wall panels. In this study, rice straw fiber was pulverized and combined with magnesium oxychloride cement (MOC) to produce a kind of RSFC with high content of straw and suitable for light steel keel wall panels. It is found that the mass content of RS in the RSFC used in the wall panel can reach about 12%. The rice straw concrete-light steel keel wall panels (RS-LSWP) proposed provides a technical means for rational utilization of RS and can promote the development of light steel residential buildings. The research results promote the application of straw and other agricultural wastes in building materials and also provide a way for the green, coordinated, and healthy development of rural areas.

2. Materials and Methods

2.1. Rice Straw Fiber Concrete

2.1.1. Raw Materials and Preparation Process

The rice straw fibers used are non-rotting, dried and crushed straw. To alleviate the problem of straw clumping, RS and husk were mixed in a mass ratio of 3:1 (Figure 1). Light-fired magnesium oxide powder (industrial magnesium oxide powder) with a content of 73.8% and magnesium sulfate crystal heptahydrate (chemical formula $\text{MgSO}_4 \cdot 7\text{H}_2\text{O}$) as the main compelling materials were used. The compound acid modifier, mainly composed of phosphoric acid, is provided by Shenyang Tianque Building Materials Co., LTD, Shenyang, China. The modifier can be used to improve the comprehensive performance of RSFC.



Figure 1. Raw material: (a) rice straw; (b) husk.

The tool used to stir RSFC is the industrial electric mixer. Before preparing the specimen, $\text{MgSO}_4 \cdot 7\text{H}_2\text{O}$ was mixed with warm water at 40 °C at a mass ratio of 1:1 to form a magnesium sulfate solution. The preparation of RSFC begins by mixing rice straw with lightly burned magnesium oxide powder through the mixer. Next, the compound acid modifier was added to the magnesium sulfate solution and then added to the mixture of RS and magnesium oxide. The mixture was thoroughly stirred and then poured into the test mold to vibrate. Finally, it was cured under natural indoor conditions. Figure 2 shows the preparation process of RSFC.

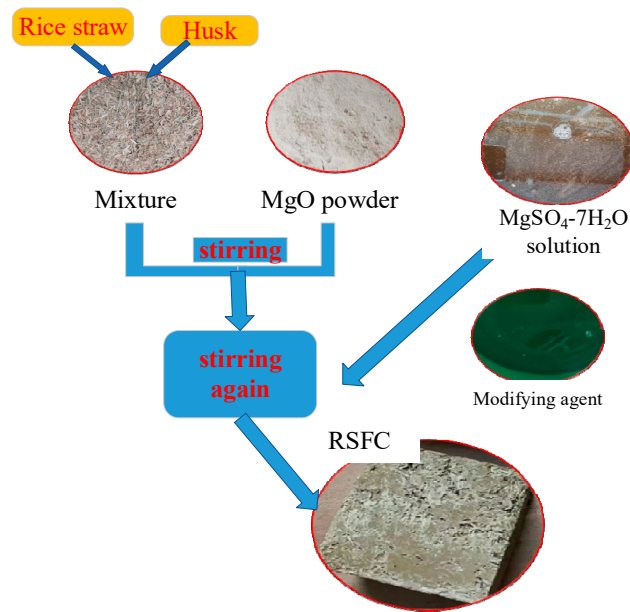


Figure 2. Flow chart.

2.1.2. Test Method

The apparent density, compressive strength test and tensile strength test of RSFC were measured according to the standard test method for mechanical Properties of ordinary Concrete GBT50081-2019 [41]. An MTS microcomputer-controlled electro-hydraulic servo universal testing machine with a range of 1000 kN was used to carry out the corresponding test, and the loading speed was 0.3 kN/s. Formulas (1)–(3) are the calculation formulas of apparent density, compressive strength and splitting strength of concrete, respectively:

$$\rho_a = \frac{m_d}{V_a} \quad (1)$$

ρ_a is the apparent density of concrete, m_d is the mass of the specimen under dry conditions, and V_a is the apparent volume of the specimen.

$$R = \frac{P}{A} \quad (2)$$

R is the standard compressive strength of RSFC(MPa), P is the ultimate load (N) at the time of failure, and A is the compression surface area (mm^2) of the RSFC.

$$R_t = \frac{2P}{\pi A} \quad (3)$$

R_t is the standard value of splitting tensile strength (MPa), P is the ultimate load (N) at the time of failure, and A is the area of the splitting surface of the cube test block of the RSFC (mm^2).

The hot-wire method (Figure 3) was used to measure the thermal conductivity of the test block. To improve the measurement accuracy, the average value of the test block was calculated after multiple measurements. The hot-wire method is an analytical method based on the proportional relationship between temperature rise ΔT and logarithmic heating time ($\ln(t)$) within a long enough time (300 s) [42].

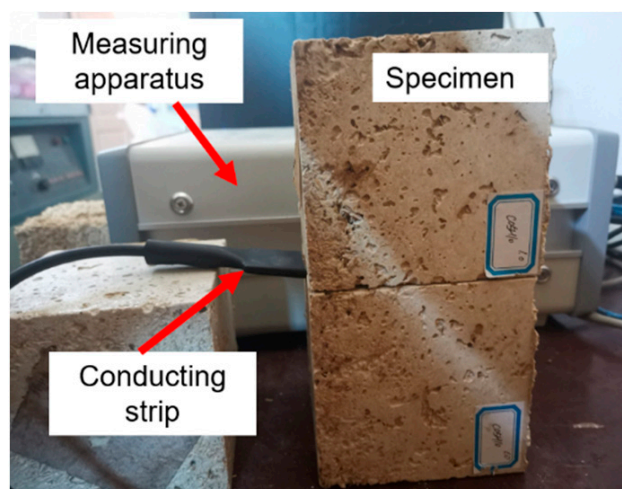


Figure 3. Thermal conductivity test.

2.1.3. Mix Ratio

Considering the influence of straw length, straw content, modifier content, and cementing material ratio, seven experimental material ratio schemes were designed for the material ratio of straw fiber concrete (Table 1).

Table 1. Material mix ratio.

| Number | MgO/MgSO ₄ /H ₂ O ^① | Modifier ^② (%) |
|--------------|--|---------------------------|
| C05H08(0.5) | 8/1/20 | 0.5 |
| C10H08(0.5) | 8/1/20 | 0.5 |
| C15H08(0.5) | 8/1/20 | 0.5 |
| C05H08(1.0) | 8/1/20 | 1.0 |
| C05H10(1.0) | 8/1/20 | 1.0 |
| C05H12(1.0) | 8/1/20 | 1.0 |
| C05H12*(1.0) | 9/1/20 | 1.0 |

^① means molar ratio, ^② mass ratio.

In Table 1, the letter C represents RS length (5 mm, 10 mm, and 15 mm), and the letter H represents RS mass content (8%, 10%, and 12%). The symbol "*" represents the ratio of MgO:MgSO₄:H₂O at 9:1:20, and the ratio of MgO:MgSO₄:H₂O is 8:1:20 without the symbol "*". The numbers 0.5 and 1.0 in brackets represent the total mass ratio of the acid modifier used to the active magnesium oxide. For example, C05H08(1.0) means that the length of RS is 5 mm, the mass content of RS and husk is 8%, the proportion of MgO:MgSO₄:H₂O of cementing material is 8:1:20, and the modifier content accounts for 1% of the total mass ratio of active magnesium oxide. The cementitious material in RSFC is proportioned by the molar mass ratio. All letters and symbols have the same meaning unless otherwise stated below.

2.2. Thermal Performance of RS-LSWP

2.2.1. Computational Theory and Model Verification

Code for thermal design of civil building GB50176-2016 [43] uses the comprehensive heat transfer coefficient of wall panels obtained by steady-state heat transfer to evaluate the thermal performance of building wall panel construction. Although ANSYS can analyze steady-state and transient heat transfer problems under various boundary conditions, it cannot directly calculate the comprehensive heat transfer coefficient of the wall panel. It is necessary to convert according to the relationship between the average heat flux and the heat transfer coefficient of the inner (outer) surface of the wall. In this study, ANSYS2019

was used to calculate the heat flux of the wall panel, and then the heat flux of each node on the inner (outer) surface of the wall panel was extracted and the average value was calculated. Formula (4) was used to calculate the comprehensive heat transfer coefficient of the wall panel.

$$K = \frac{q}{\Delta t} \quad (4)$$

K is the wall comprehensive heat transfer coefficient ($\text{W}/\text{m}^2\cdot\text{K}$), q is the average heat flux of the inner (outer) surface of the wall (W/m^2), and Δt is the temperature difference between the inner and outer surfaces of the wall (K or $^{\circ}\text{C}$).

In the finite element model, PLANE55 is used to simulate steel keel, RSFC, wood strip, and rock wool. Because the thermal contact resistance between various materials of the enclosure structure has little influence on the thermal performance of the wallboard, this study does not consider this influence.

To verify the accuracy of model simulation results, taking Harbin as an example, the finite element calculation results of a 500 mm thick single material layer and 125 mm + 250 mm + 125 mm two material layers (Figure 4) were compared with the theoretical calculation results recommended by Chinese national specification GB50176-2016. The calculated temperatures indoors and outdoors are 18°C and -26°C , respectively. The surface heat transfer coefficients of interior and exterior walls are found to be $8.7 \text{ W}/(\text{m}^2\cdot\text{K})$ and $23.0 \text{ W}/(\text{m}^2\cdot\text{K})$, respectively, taking into account convective heat transfer and radiation heat transfer. The thermal conductivity of steel keel is $58.2 \text{ W}/(\text{m}\cdot\text{K})$, that of rock wool is $0.05 \text{ W}/(\text{m}\cdot\text{K})$, that of straw concrete is $0.086 \text{ W}/(\text{m}\cdot\text{K})$ and that of OBS is $0.17 \text{ W}/(\text{m}\cdot\text{K})$. Unless otherwise specified in the following section, the related parameters are the same as those in this section. Table 2 shows the comparison results. The calculation error of the model is within 2%, indicating high accuracy of the simulation.

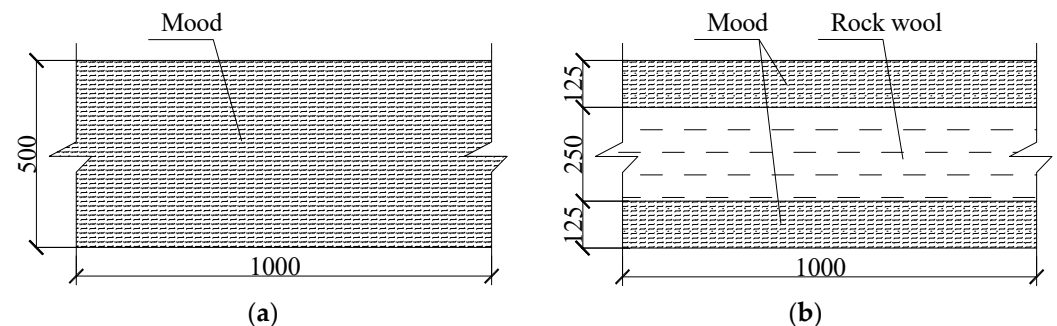


Figure 4. Finite element model scheme: (a) 0.5 m single-story wooden structure; (b) Double timber construction with rock wool.

Table 2. Comparison of finite element simulation and theoretical calculation.

| Computational Model | Theoretical Calculation ($\text{W}/\text{m}^2\cdot\text{K}$) | Finite Element Simulation ($\text{W}/\text{m}^2\cdot\text{K}$) | Error (%) |
|--|---|---|-----------|
| 0.5 m single-story wooden structure | 0.322 | 0.327 | 1.5 |
| Double timber structure with rock wool | 0.1509 | 0.1509 | 0 |

2.2.2. Parameterization

Four different light steel keel structural forms, including type C, antitype C, type Z and inverted type Z, were designed (Figure 5). Considering the effects of the height of the web depth, the width of the flange, and the offset distance of the opposite keel, the parametric analysis was carried out. To ensure the principle of single-variable analysis parameters, the walls used in this paper are all in the form of 12 mm OSB + 300 mm RSFC + 12 mm OSB.

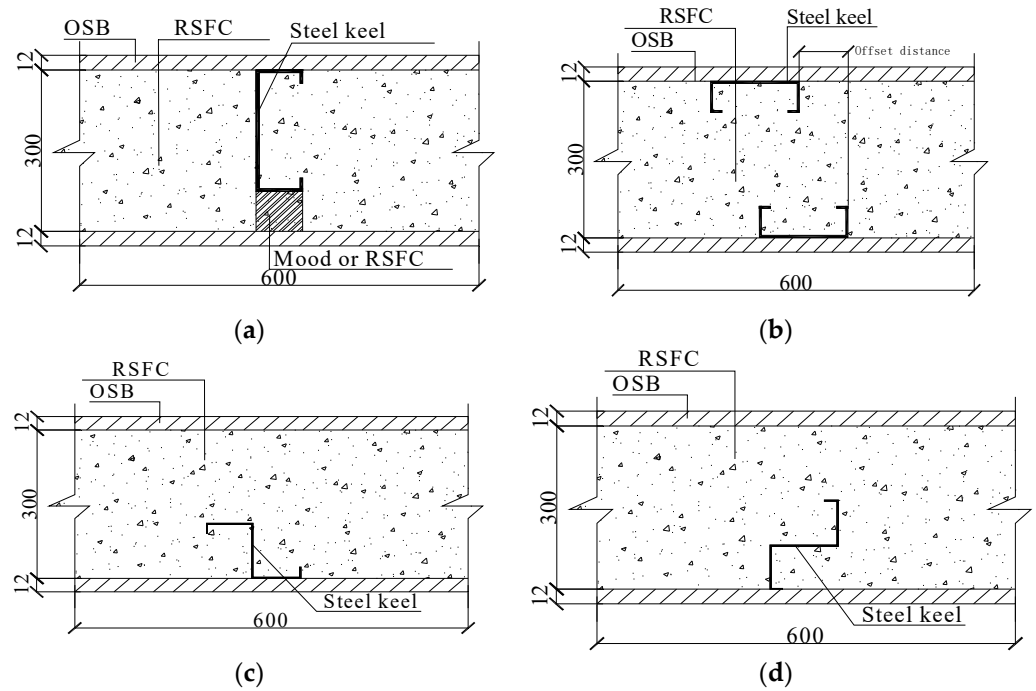


Figure 5. Parameterized model: (a) Type C; (b) Antitype C; (c) Type Z; (d) Inverted type Z.

3. Results and Discussion

3.1. Rice Straw Fiber Concrete

3.1.1. Compressive Strength

The compressive strength of the RSFC was measured after curing it for 1, 3, 7, 14 and 28 days under natural indoor conditions. The standard compressive strength of RSFC was obtained by multiplying the compressive strength of the cube by the conversion coefficient of strength size 0.95. It can be found that with the increase in RS length, the standard compressive strength of RSFC first decreases and then increases, and the standard compressive strength of RSFC reaches the maximum when the RS length is 0.5 cm (Figure 6a). The higher the content of RS, the lower the strength of RSFC (Figure 6b). When the content of the modifier increases from 0.5% to 1.0%, the standard compressive strength of RSFC increases (Figure 6c). When the ratio of MgO:MgSO₄:H₂O changes from 8:1:20 to 9:1:20, the standard compressive strength of RSFC decreases (Figure 6d). In addition, the standard value of the 14-day compressive strength of RSFC reached about 85% of the standard value of the 28-day compressive strength.

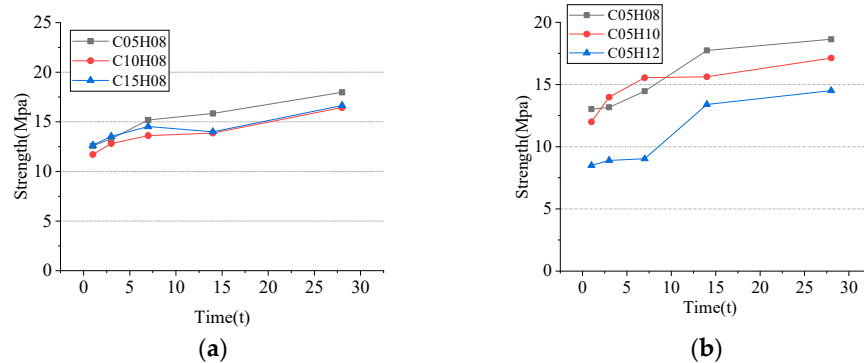


Figure 6. Cont.

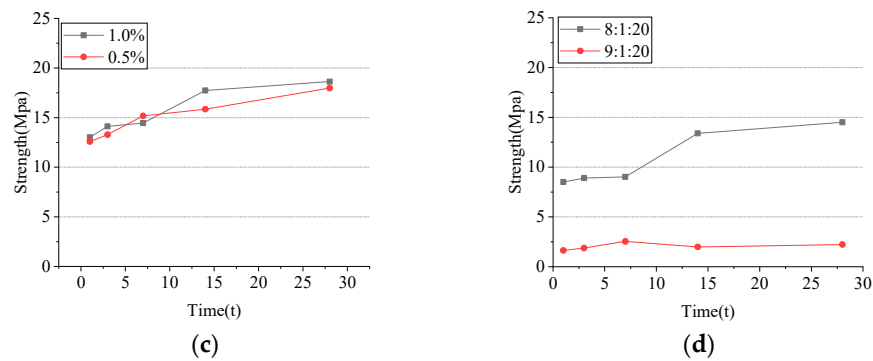


Figure 6. Standard compressive strength of RSFC with different proportions: (a) Different RS lengths; (b) Different RS content; (c) Modifiers with different contents; (d) Cementitious materials with different proportions.

3.1.2. Tensile Strength

Table 3 shows the 28-day tensile strength results of the RSFC specimen. It can be found that the increase in the content of the modifier has a certain effect on the standard tensile strength of RSFC. The higher the content of RS, the lower the standard tensile strength of RSFC. When the ratio of $\text{MgO}:\text{MgSO}_4:\text{H}_2\text{O}$ changes from 8:1:20 to 9:1:20, the standard tensile strength of RSFC decreases.

Table 3. Standard tensile strength of RSFC with different proportions.

| Number | Strength (Mpa) |
|--------------|----------------|
| C05H08(0.5) | 1.74 |
| C05H08(1.0) | 1.98 |
| C05H10(1.0) | 1.68 |
| C05H12(1.0) | 1.42 |
| C05H12*(1.0) | 0.64 |

3.1.3. Thermal Conductivity

Table 4 shows the thermal conductivity of three groups of RSFC with different mix ratios. It can be found that when the molar mass ratio of $\text{MgO}:\text{MgSO}_4:\text{H}_2\text{O}$ is 8:1:20, the thermal conductivity of RSFC is larger, and the different proportions of cementing materials have a great influence on the thermal conductivity of the straw concrete. The thermal conductivity of the straw concrete with the molar mass ratio of 9:1:20 $\text{MgO}:\text{MgSO}_4:\text{H}_2\text{O}$ is 0.0862 $\text{W}/(\text{m}\cdot\text{K})$, which meets the requirements of the thermal conductivity of thermal insulation materials stipulated by the national code (GB50176-2016).

Table 4. Thermal conductivity of RSFC.

| Number | Thermal Conductivity ($\text{W}/(\text{m}\cdot\text{K})$) |
|--------------|---|
| C05H08(1.0) | 0.617 |
| C05H10(1.0) | 0.600 |
| C05H12*(1.0) | 0.0862 |

3.1.4. Density and Surface Cracks

This study measured the apparent density and observed the surface cracks of RSFC with different proportions after 28 days of curing. The results show that the higher the RS content, the lower the RSFC density. When the ratio of $\text{MgO}:\text{MgSO}_4:\text{H}_2\text{O}$ changed from 8:1:20 to 9:1:20, the density of RSFC decreased to a large extent (Figure 7). Figure 8 shows the surface cracks of the straw concrete specimen. It can be found that when the RS content is less than 10%, the surface of the RSFC is easy to crack, which may be related to

the volume expansion of the RSFC caused by the reaction of the active magnesium oxide with water which forms magnesium hydroxide during the condensation and hardening process of magnesium oxide and magnesium sulfate. However, when the straw content is 12%, the volume expansion generated by the magnesium hydroxide in the test block can be released in the gap due to the increase in RS content, and there are almost no cracks on the concrete surface. Thus, to avoid cracks, the content of RSFC should be more than 12%.

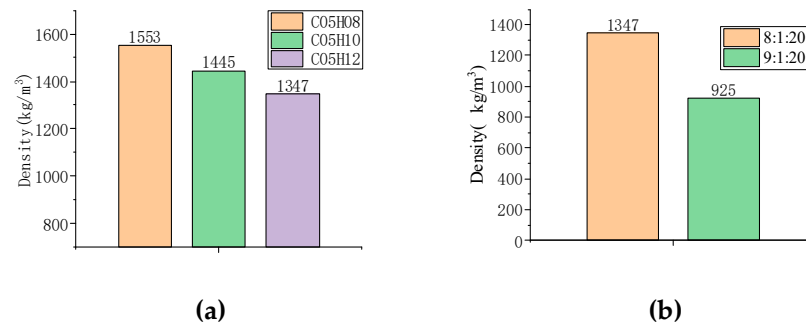


Figure 7. RSFC density: (a) Different RS content; (b) Different proportions of cementitious materials.

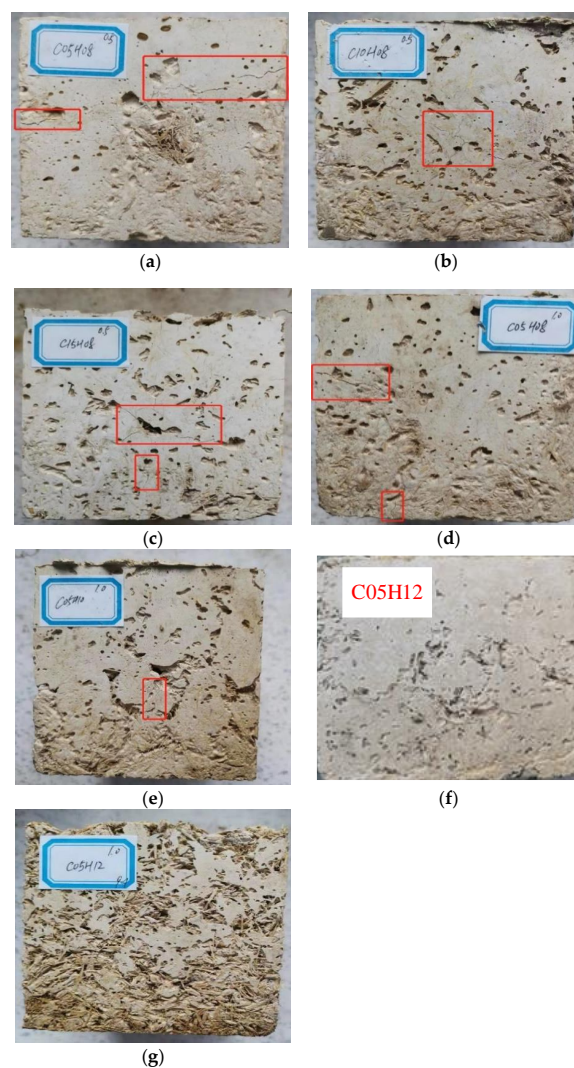


Figure 8. Surface crack (red box): (a) C05H08(0.5); (b) C10H08(0.5); (c) C15H08(0.5); (d) C05H08(1.0); (e) C05H10(1.0); (f) C05H12(1.0); (g) C05H12*(1.0).

Based on the above analysis, considering the RSFC cost, surface crack, density and insulation performance, it is recommended to adopt the RS ratio of 5 mm straw length, 12% mass content, 8:1:20 mass ratio of MgO:MgSO₄:H₂O, and 1% conditioner content for RS-LSWP. The standard compressive strength, tensile strength, and thermal conductivity of the mixture are 2.2 MPa, 0.64 MPa, and 0.0862 W/(m·K), respectively. The mass content of various materials per cubic meter of concrete under this mix ratio is shown in Table 5.

Table 5. Straw concrete ratio.

| Composition | Content (kg/m ³) |
|--------------------------------------|------------------------------|
| Rice straw | 81 |
| Husk | 27 |
| Magnesium oxide | 340 |
| MgSO ₄ •7H ₂ O | 235 |
| Modifier | 2.65 |

3.2. Thermal Performance of RS-LSWP

3.2.1. Type C

- Influence of different web widths on the thermal performance of RS-LSWP

The structure diagram of the RS-LSWP is shown in Figure 5a. Figure 9 shows the temperature field of the RS-LSWP when the web width of the steel keel is 100 mm, 150 mm, 200 mm, 250 mm and 300 mm, respectively. When the web width of the steel keel is below 150 mm, the influence range of the cold bridge effect of the steel keel gradually expands with the increase in web width. When the web width of the steel keel is greater than 200 mm, the cold bridge effect decreases with the increase in web width. Hence, the keel flange spacing should be more than 200 mm.

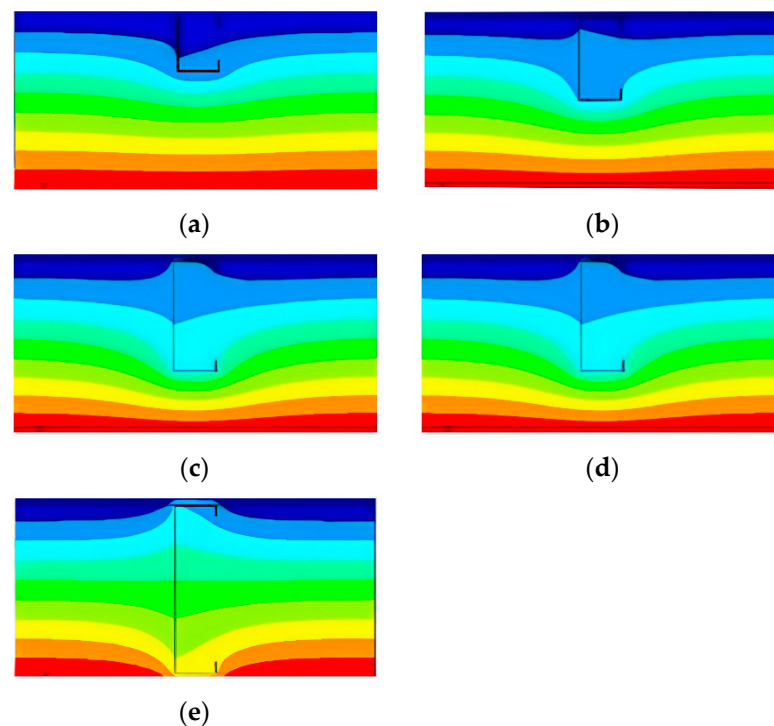


Figure 9. Temperature field of RS-LSWP: (a) 100 mm; (b) 150 mm; (c) 200 mm; (d) 250 mm (e) 300 mm.

Figure 10 shows the variation rule of wall panel internal surface temperature with different web widths. It can be found that with the increase in the web width in the wall panel, the difference between the temperature of the inner surface of the wall and the

surrounding temperature also gradually increases. When the height of the web width is 300 mm, there is a significant difference between the temperature at the cold bridge position and the surrounding temperature, which can reach 7~8 °C. Hence, the cold bridge effect can be significantly reduced by using a steel keel structure that does not penetrate the wall panel.

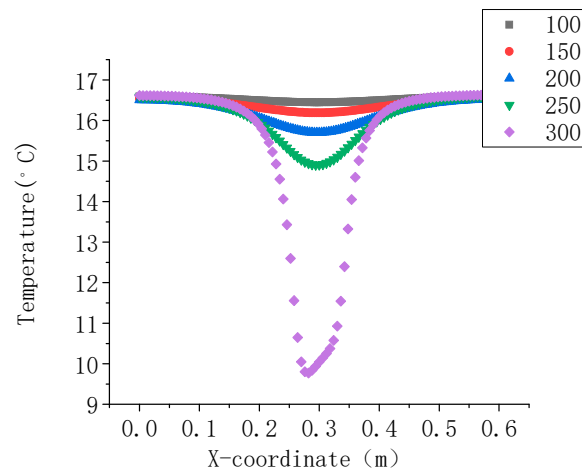


Figure 10. Internal surface temperature variation curve of type C wall panel in different insulation forms.

- Influence of different insulation forms on the thermal performance of RS-LSWP

The thermal performance of the RS-LSWP was analyzed considering the insulation forms of internal and external insulation and whether the steel keel and OSB board were padded with battens. It can be found that compared with external insulation, the internal surface temperature variation rule of the internal insulation wall panel is not affected by the keel cold bridge effect. The internal surface temperature variation trend of steel keel walls is almost the same as that of straw concrete internal insulation and batten internal insulation. This indicates that the keel cold bridge effect of steel keel does not influence the temperature change in the inner surface of the wall. In addition, the results show that the insulation effect of RS is better than that of batten (Figures 11 and 12).

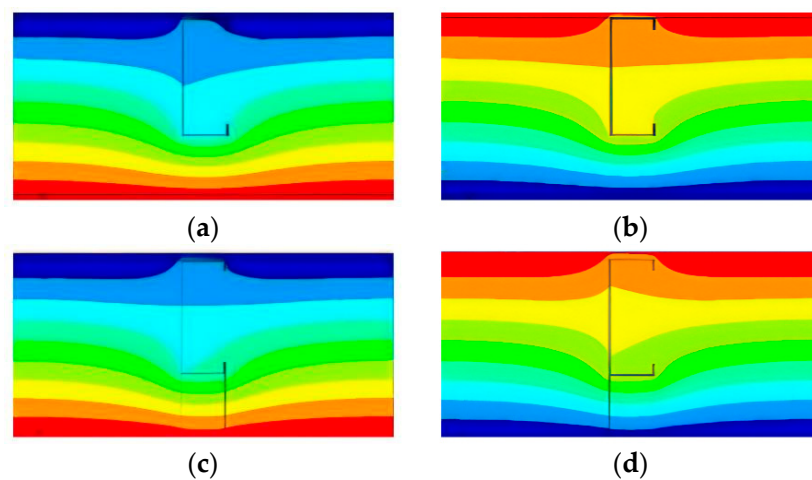


Figure 11. Temperature field of RS-LSWP in different insulation forms: (a) RS internal insulation; (b) RS external insulation; (c) Fill battens for internal insulation; (d) Fill battens for external insulation.

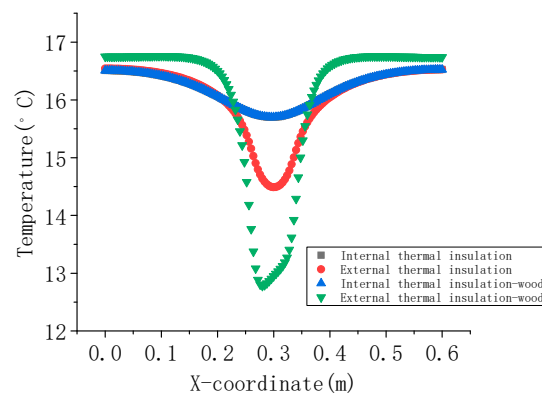


Figure 12. Internal surface temperature variation curve of type C in different insulation forms.

- Comprehensive heat transfer coefficient of RS-LSWP with different web widths and different insulation forms

GB50176-2016 requires that the comprehensive heat transfer coefficient of the external wall in different cold areas is not higher than a certain value. The influence of different web widths of steel keel on the comprehensive heat transfer coefficient is analyzed. Figure 13 shows that the comprehensive heat transfer coefficient of the wall panel increases with the increase in the web depth. When the steel keel does not penetrate the wall panel, the comprehensive heat transfer coefficient of the wall panel increases slowly, but when the keel penetrates the wall panel, the heat transfer coefficient increases. The effect of external insulation is better than that of internal insulation, but the distinction is not obvious. Battens will degrade the thermal performance of the wall panel. Hence, considering the indoor living comfort of the occupant and to prevent the condensation phenomenon, for this kind of wall panel, the internal insulation scheme should be preferred.

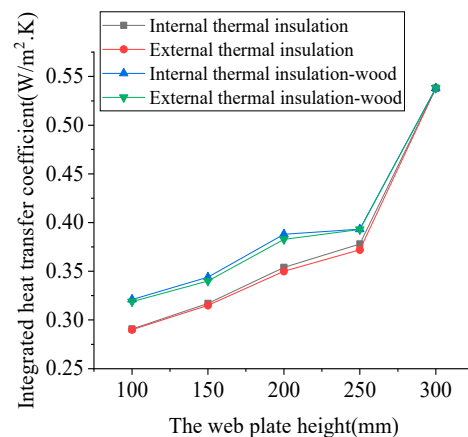


Figure 13. Comprehensive heat transfer coefficient curves of type C with different web depths and different insulation forms.

3.2.2. Antitype C

- Influence of different flange heights on the thermal performance of RS-LSWP

Considering the steel keel flange heights of 40 mm, 50 mm, 60 mm, and 70 mm, the thermal performance of the RS-LSWP was analyzed and parameterized. The structure diagram of the wall panel is shown in Figure 5b. The results of the temperature field calculation show that the influence range of the cold bridge effect of the steel keel expands gradually with the increase in flange height, but the influence range of the cold bridge effect of one side of the steel keel does not extend to the other side. The cross-section form of the antitype C steel keel can effectively reduce the transmission of the keel cold bridge

effect in the thickness direction of the wall panel (Figure 14). Meanwhile, with the increase in the height of the steel keel flange, the minimum temperature of the inner surface of the wall panel decreases gradually. However, the phenomenon of the cold bridge is not obvious; the temperature of the inner surface of the wall panel is less than 2 °C, which is lower than the temperature around the wall. This means that an increase in the width of the steel keel flange does not change the range of temperature in the inner surface of the wall panel (Figure 15).

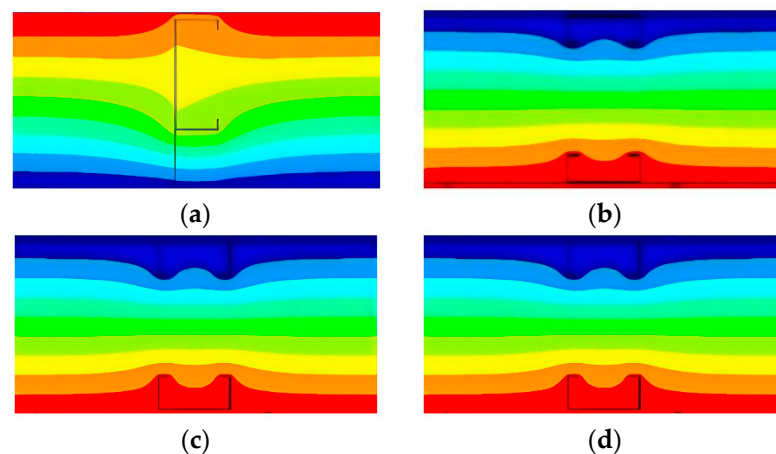


Figure 14. Temperature field of different flange heights in antitype C: (a) 40 mm; (b) 50 mm; (c) 60 mm; (d) 70 mm.

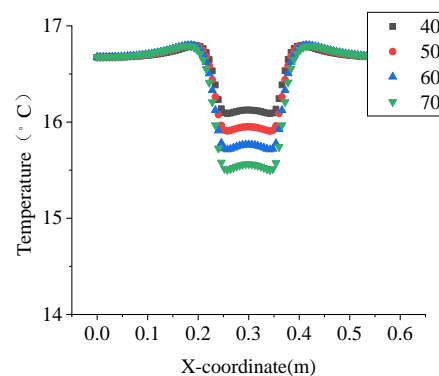


Figure 15. Internal surface temperature curves of different flange widths in antitype C.

- Influence of different offset distances on the thermal performance of RS-LSWP

The thermal performance of the RS-LSWP is analyzed considering that the opposite offset distance of the steel keel is 0 mm, 30 mm, 60 mm and 90 mm, respectively. The calculation results of the temperature field show that the cold bridge displacement of the steel keel is also offset by the increase in the opposite displacement distance of the steel keel. The offset of the opposite side of the steel keel has reduces the cold bridge effect of the keel (Figure 16). In addition, with the increase in the offset distance of the opposite side of the steel keel, the inner surface of the wall panel hardly changed. The phenomenon of the cold bridge effect of steel keel is not obvious, and the lowest temperature on the inner surface of the wall panel is only less than 2 °C lower than the temperature around (Figure 17).

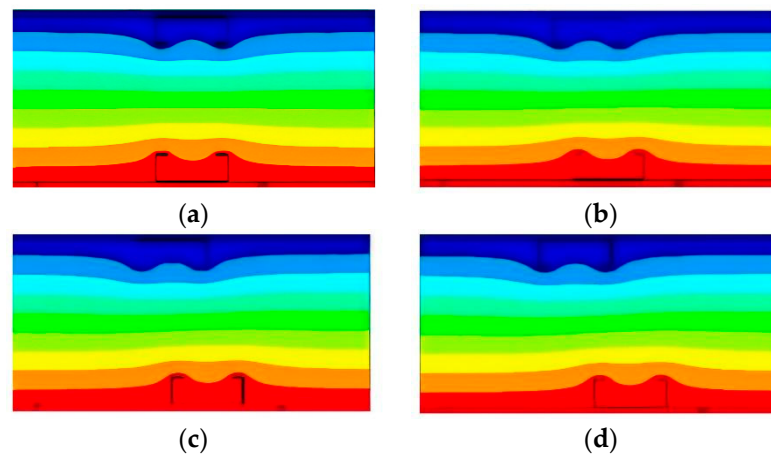


Figure 16. Temperature field with different offset distances in antitype C: (a) 0 mm; (b) 30 mm; (c) 60 mm; (d) 90 mm.

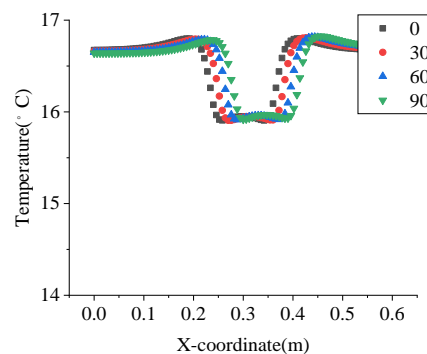


Figure 17. Internal surface temperature curves of different offset distances in antitype C.

- Comprehensive heat transfer coefficient analysis of wall panels with different flange heights and different offset distances

Figure 18 shows the influence of different flange heights and different offset distances on the comprehensive heat transfer coefficient of the steel keel. It can be found that the comprehensive heat transfer coefficient of the wall panel is not related to the opposite offset distance but to the flange height. The comprehensive heat transfer coefficient of the wall panel increases obviously with the increase in flange height. When the flange height of the steel keel is 40 mm, the comprehensive heat transfer coefficient of the wall panel is about $0.28 \text{ W}/(\text{m}^2 \cdot \text{K})$. However, when the flange height of the steel keel increases to 70 mm, the comprehensive heat transfer coefficient of the wall panel is about $0.31 \text{ W}/(\text{m}^2 \cdot \text{K})$.

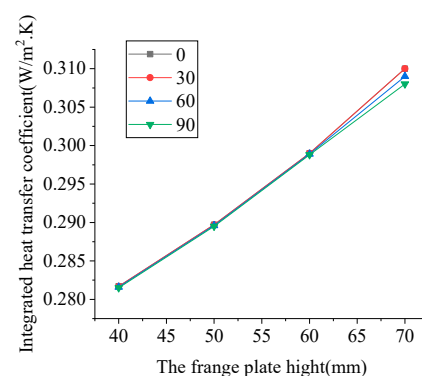


Figure 18. Comprehensive heat transfer coefficient curve in antitype C.

3.2.3. Type Z

- Influence of different web widths on the thermal performance of RS-LSWP

The thermal performance of the internal thermal insulation wall panel was analyzed considering that the web width is 100 mm, 150 mm, 200 mm, 250 mm, and 300 mm, respectively. The structure diagram of the wall panel is shown in Figure 5c. The results of temperature field calculation show that when the web width of the steel keel is less than 150 mm, the influence range of the cold bridge effect of the steel keel gradually expands with the increase in web widths. When the height of the steel keel web is greater than 200 mm, the influence range of the steel keel cold bridge effect decreases gradually with the increasing distance of the keel flange. This is mainly because with the increase in the flange distance of the steel keel, the cold bridge effect of the keel gradually can only be transmitted by the web. Therefore, the flange distance should be more than 200 mm. This is consistent with the temperature variation law of type C (Figure 19). The temperature curve shows that with the increase in steel keel web height, the minimum temperature of the inner surface of the wall panel decreases gradually, and the influence range of the cold bridge effect temperature of the steel keel expands gradually. When the web height of the steel keel is 300 mm, the inner surface temperature of the steel keel decreases, and the influence range of temperature expands. The use of a non-penetrating steel keel structure is conducive to reducing the cold bridge effect of the keel and increasing the inner surface temperature of the wall panel (Figure 20).

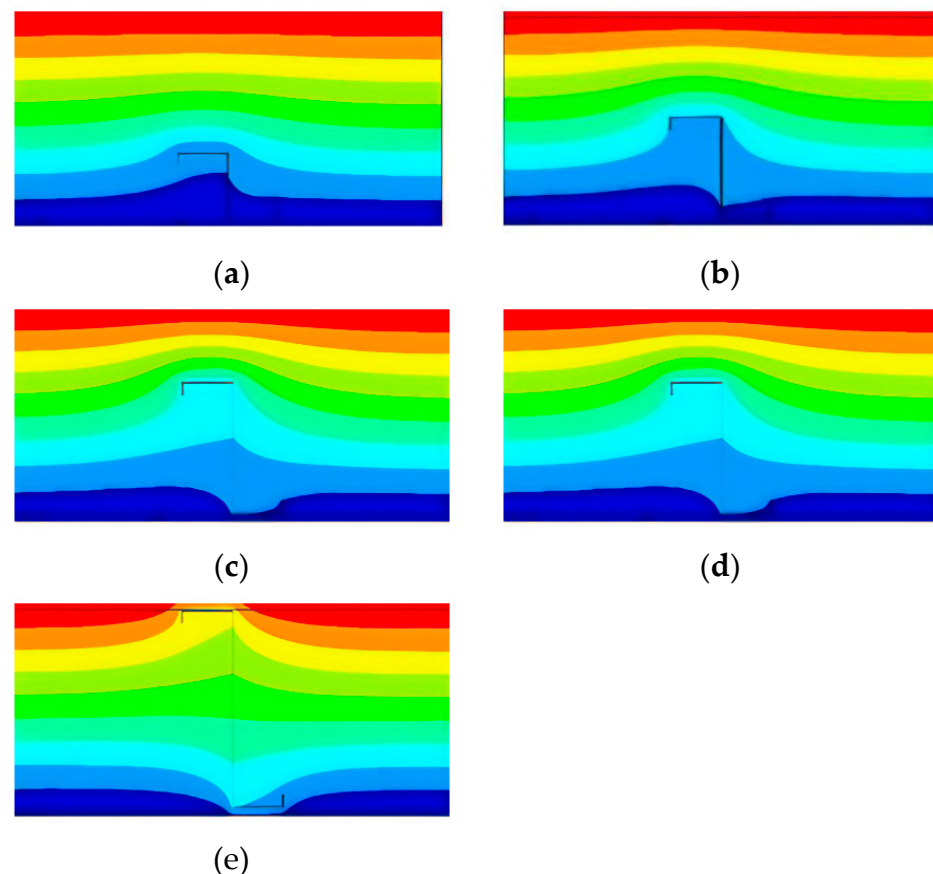


Figure 19. Temperature field with different web heights in type Z: (a) 100 mm; (b) 150 mm; (c) 200 mm; (d) 250 mm; (e) 300 mm.

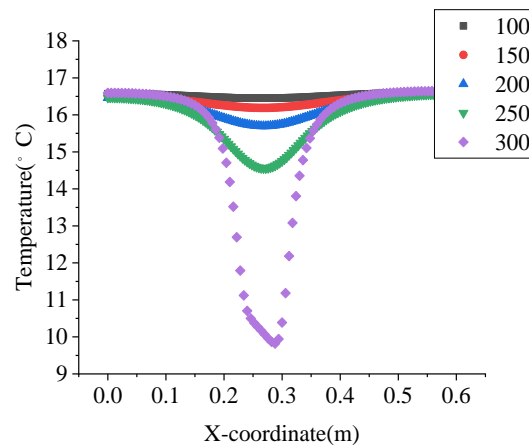


Figure 20. Internal surface temperature curves of different web heights in type Z.

- Comprehensive heat transfer coefficient analysis of wall panels with different flange heights and different offset distances

Figure 21 shows the influence curve of web widths of type Z steel keel section on the comprehensive heat transfer coefficient of the internal insulation wall panel. The results show that the comprehensive heat transfer coefficient of the wall panel increases with the increase in the height of the steel web, and the comprehensive heat transfer coefficient of the wall panel is $0.304 \text{ (W/m}^2\cdot\text{K)}$ when the height of the web is 100 mm. When the web height increases to 300 mm, the comprehensive heat transfer coefficient of the wall panel is $0.5381 \text{ (W/m}^2\cdot\text{K)}$. The width of the web has a great influence on the comprehensive heat transfer coefficient of the wall panel.

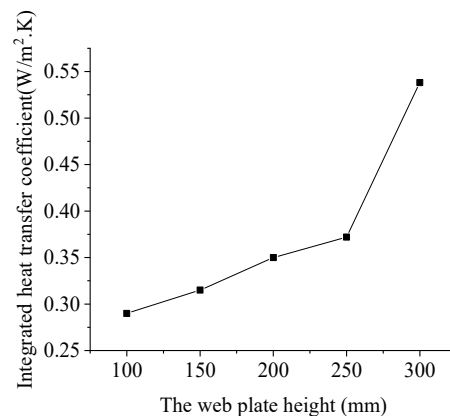


Figure 21. Comprehensive heat transfer coefficient curve in type Z.

3.2.4. Inverted Type Z

- Influence of different flange widths on the thermal performance of RS-LSWP

The thermal performance of the steel keel was analyzed with flange widths of inverted Z section of 75 mm, 100 mm, 125 mm and 150 mm, respectively. The construction diagram of the wall panel is shown in Figure 5d. With the increase in flange height of inverted type Z, the influence range of the cold bridge effect of the steel keel decreases gradually. The cold bridge effect has the largest influence range at 75 mm. With the increase in flange height, the influence of the web on the cold bridge effect decreases gradually. Thus, the flange height should be more than 100 mm (Figure 22). Meanwhile, with the increase in the height of the steel keel flange, the inner surface temperature of the steel keel wall panel gradually decreases, and the influence range of the keel flange on the inner surface temperature gradually expands. When the total flange height reaches 300 mm, the influence range of the

temperature of the steel keel on the inner surface temperature of the wall panel increases. Therefore, for this form, non-penetrating steel keel sections should be selected (Figure 23).

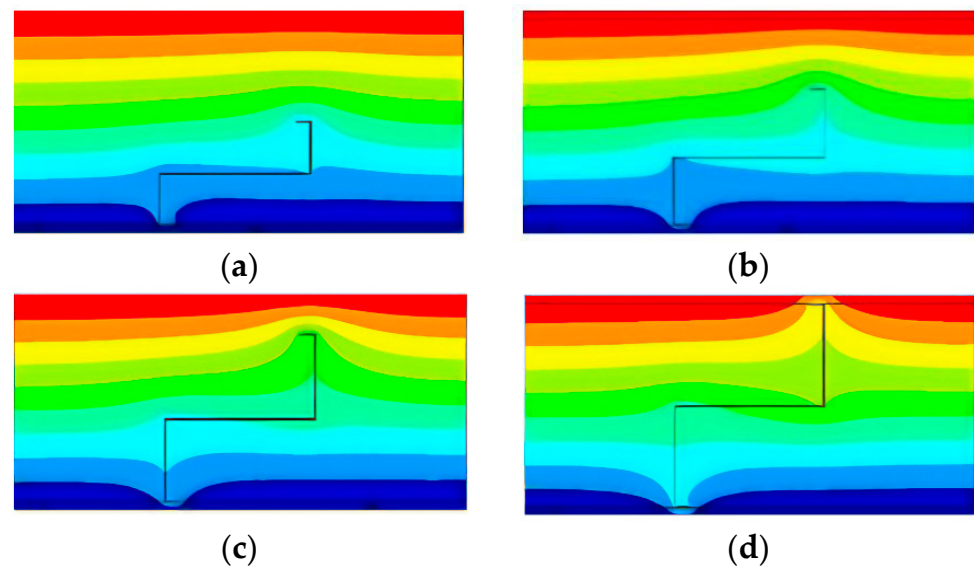


Figure 22. Temperature field with different flange widths in inverted type Z: (a) 75 mm; (b) 100 mm; (c) 125 mm; (d) 150 mm.

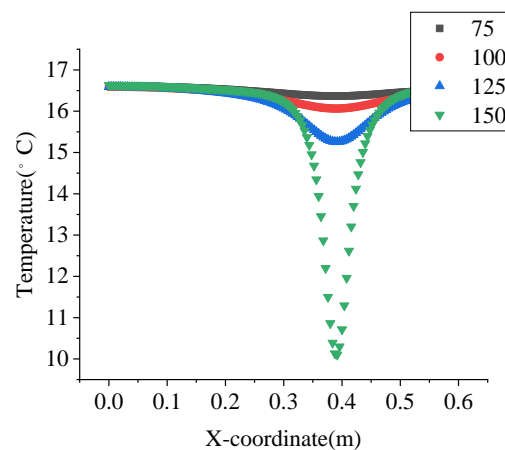


Figure 23. Internal surface temperature curves of different flange widths in inverted type Z.

- Influence of different web widths on the thermal performance of RS-LSWP

Considering that the height of the steel keel section web is 100 mm, 150 mm, 200 mm, 250 mm and 300 mm, respectively, the thermal performance of the wall panel is analyzed. The structure diagram of the wall panel is shown in Figure 5d. The results of temperature field calculation show that with the increase in web height of the steel keel, the influence range of the steel keel cold bridge effect increases gradually in the web height range, but decreases gradually in the flange width range. When the height of the web is above 250 mm, the cold bridge effect at the flange of the keel in the wall panel significantly decreases, and the influence range of the cold bridge effect of the keel also gradually decreases (Figure 24). The curve shows that the influence of the cold bridge effect on the inner surface temperature of the wall panel is unchanged because the steel keel is located outside of the wall panel. The increase in the web height of the steel keel does not affect the temperature variation rule of the inner surface of the wall panel (Figure 25).

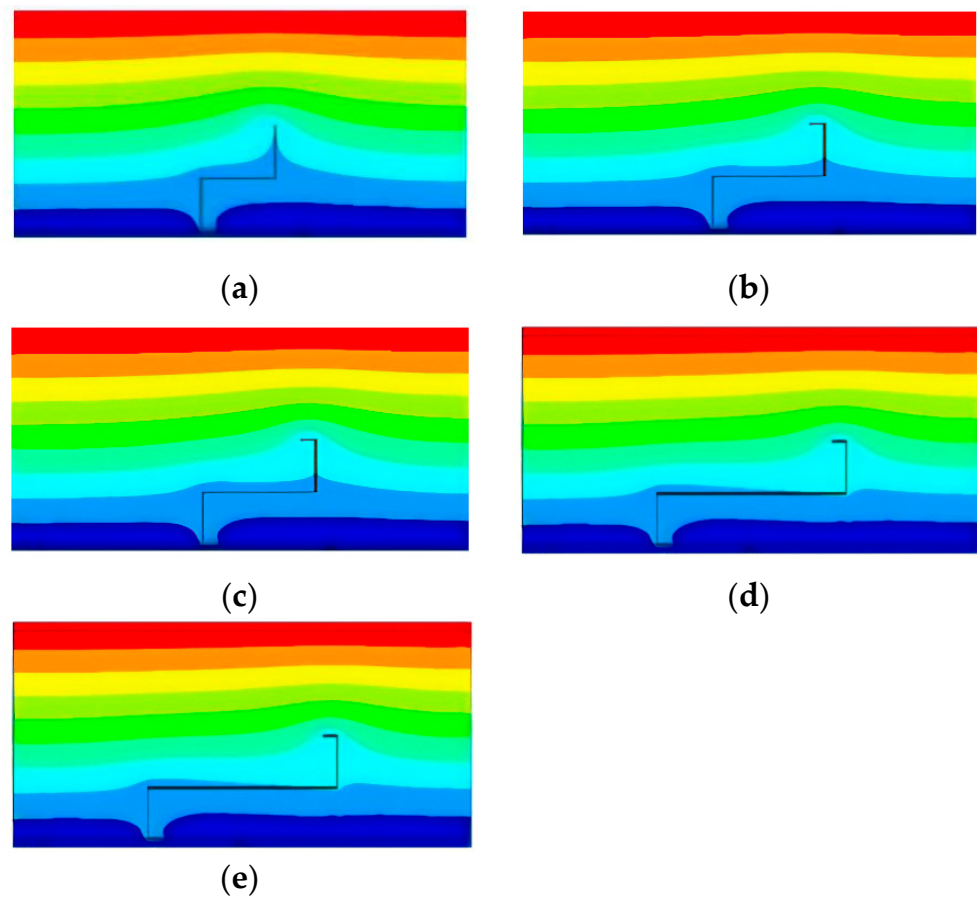


Figure 24. Temperature field with different web heights in inverted type Z: (a) 100 mm; (b) 150 mm; (c) 200 mm; (d) 250 mm; (e) 300 mm.

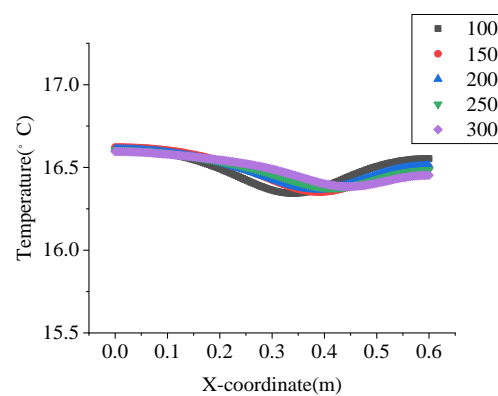


Figure 25. Internal surface temperature curves of different web heights in inverted type Z.

- Comprehensive heat transfer coefficient analysis of wall panels with different web widths and flange heights

Figure 26 shows the influence of different web heights and flange widths of inverted Z section steel keel on the comprehensive heat transfer coefficient of the wall panel. The results show that with the increase in the height of the steel keel web, the comprehensive heat transfer coefficient of the wall panel decreases gradually. The comprehensive heat transfer coefficient of wall panels with flange widths of 75 mm, 100 mm and 125 mm decreases slowly, while that with a flange width of 150 mm decreases rapidly. This is mainly because the keel with a width of 150 mm flange runs through the thickness of the

wall panel, and the keel cold bridge effect is obvious. Therefore, for such a keel arrangement form, a non-penetrating steel keel arrangement is better.

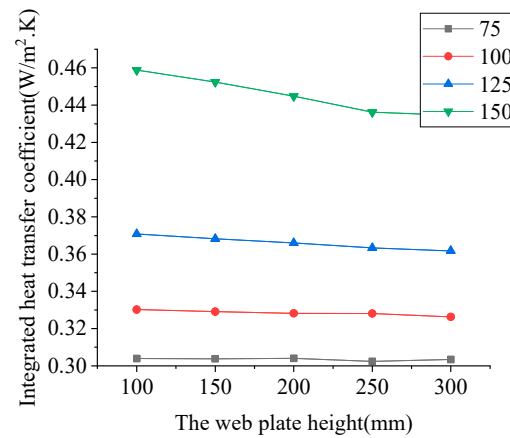


Figure 26. Comprehensive heat transfer coefficient curve of inverted type Z with different web heights and flange lengths.

3.2.5. Comparison of Thermal Performance of Different Steel Keel Structures

The comprehensive heat transfer coefficient and internal surface temperature of the four different keel arrangements were studied using quantitative comparative analysis. To ensure the principle of a single variable, the cross-section areas of different steel keel arrangements are calculated and analyzed. The results show that the inverted type Z and the antitype C keel structure can reduce the comprehensive heat transfer coefficient and improve the temperature variation law of the inner surface of the wallboard. Compared with the inverted type Z, the minimum temperature of the inner surface of the antitype C is higher, and the cold bridge phenomenon is the least obvious. Therefore, antitype C is the best keel arrangement scheme in the RS-LSWP (Figure 27).

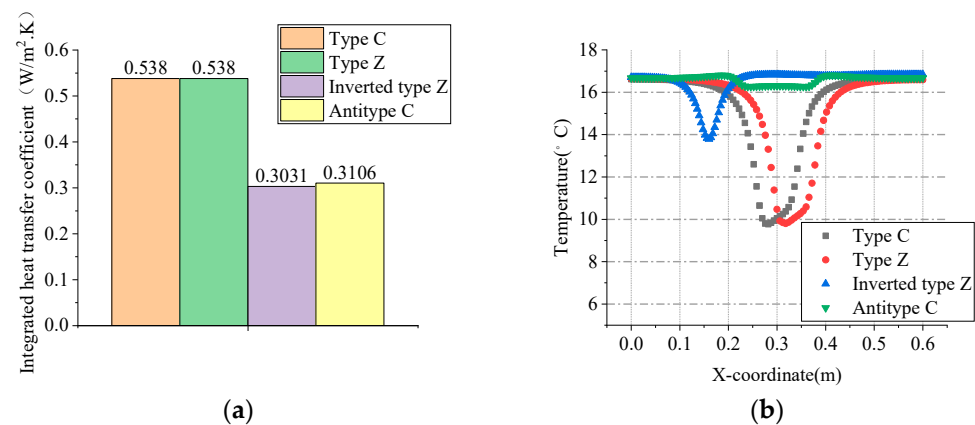


Figure 27. Comparison of thermal performance: (a) Comprehensive heat transfer coefficient; (b) Variation curve of inner surface temperature.

3.3. Discussion

To promote the rational utilization of crop fibers, such as rice straw, this study tries to combine rice straw and rice husk with magnesium cementitious material to develop an RSFC with high rice straw content and good physical and mechanical properties. The physical and mechanical properties, such as compressive strength, tensile strength and thermal conductivity of RSFC with different proportions were studied. In order to promote the practical application of RSFC, four different light steel keel structural forms are put

forward in the light steel housing. The thermal performance of these wall panels is analyzed and some properties are discovered.

The physical and mechanical properties of RSFC are significantly affected by the change in RS content and length or the difference of cementing material ratio. When the length of RS increased from 5 mm to 15 mm, the tensile strength and compressive strength of RSFC first decreased and then increased. The higher the content of RS, the lower the compressive strength of RSFC. When the content is 12% of RS, the tensile strength and compressive strength of RSFC decrease. When the modifier increased from 0.5% to 1.0%, the tensile strength and compressive strength of RSFC increased. When the ratio of MgO:MgSO₄ changes from 8:1 to 9:1, the tensile strength and compressive strength of RSFC decrease. The 14-day strength of the RSFC reaches more than 85% of the final strength. Also, the higher the RS content, the lower the RSFC density. The ratio of MgO:MgSO₄:H₂O changed from 8:1:20 to 9:1:20, and the density of RSFC decreased to a large extent. However, when the straw content is 12%, the volume expansion generated by magnesium hydroxide in the test block can be released in the gap due to the increase in RS content, and there are almost no cracks on the concrete surface.

It is recommended to adopt the RS ratio of length 5 mm, mass content 12%, the mass ratio of MgO:MgSO₄:H₂O 8:1:20, and conditioner content 1% for RS-LSWP. The standard compressive strength, tensile strength, and thermal conductivity of the mixture are 2.2 MPa, 0.64 MPa, and 0.0862 W/(m·K), respectively. Compared with the results of previous studies [32], the straw content in RSFC was greatly improved using a simpler treatment method proposed in this study. Although the mechanical properties and thermal insulation properties of RSFC are lower than those of SMLCS to a certain extent, it does not affect the popularization and application of RSFC in certain scenarios. Rock wool and foamed concrete are commonly used as fillings in light steel housing wall panels [26–32,44]. The thermal conductivity of rock wool is 0.04 W/(m·K), but the strength is close to zero [43]. The thermal conductivity of foamed concrete is above 0.5 W/(m·K), and the compressive strength is about 0.65 MPa [43]. RSFC has good thermal conductivity and the highest strength. To sum up, RSFC has certain application prospects.

Further, to study and optimize the thermal performance of RS-LSWP, four different light steel keel structural forms, including type C, antitype C, type Z and inverted type Z were designed. The influences of the height of the web depth, the width of the flange, and the offset distance of the opposite keel on the internal temperature field of the wall panel, the variation law of the temperature on the inner and outer surfaces of the wall panel and the comprehensive heat transfer coefficient are discussed. Finally, to compare the advantages and disadvantages of the four keel construction methods, the comprehensive heat transfer coefficient and internal surface temperature of the four different keel arrangements were studied using a quantitative comparative analysis. The result shows that the inverted type Z and the antitype C keel structure can reduce the comprehensive heat transfer coefficient and improve the temperature variation law of the inner surface of the wallboard. Antitype C is the best keel arrangement scheme in the RS-LSWP.

4. Conclusions

To promote the rational application of RS, reduce environmental pollution, and improve the conditions of rural housing, the physical and mechanical properties of RSFC with different proportions were studied, and the suitable mix ratio of RSFC was selected in this paper. The thermal properties of four different types of RS-LSWPs with straw concrete were simulated using the finite element software. The main conclusions are as follows:

1. The mechanical properties of RSFC can be improved by increasing the length of RS and the content of the modifier. The mechanical properties of RSFC decreased with the increase in straw content and with the mix of MgO and MgSO₄. When RS content is 12%, the compressive strength, tensile strength, apparent density, and thermal conductivity of straw concrete are reduced significantly, and the crack can be avoided effectively. The 14-day strength of RSFC reached more than 85% of the final strength.

2. The ratio of RSFC applied in RS-LSWP should be $C_{05}H_{12}^*(1.0)$. The standard compressive strength, tensile strength, and thermal conductivity of the mixture are 2.2 MPa, 0.64 MPa, and 0.0862 W/(m·K), respectively.
3. The inverted type Z and the antitype C keel structure can reduce the comprehensive heat transfer coefficient and improve the temperature curve of the inner surface of the wall panel. The antitype C keel structure is most suitable for RS-LSWP.

Author Contributions: Investigation, Y.W. (Yuqi Wu) and Y.W. (Yunqiang Wu); Data curation, Y.W. (Yunqiang Wu); Writing—original draft preparation, Y.W. (Yuqi Wu); Writing—review and editing, Y.W. (Yunqiang Wu) and Y.W. (Yue Wu); Visualization, Y.W. (Yuqi Wu) and Y.W. (Yunqiang Wu); Supervision, Y.W. (Yue Wu); Project administration, Y.W. (Yue Wu); Funding acquisition, Y.W. (Yue Wu). All authors have read and agreed to the published version of the manuscript.

Funding: This research was funded by the National Key R&D Program of China, grant number 2019YFD1101004.

Institutional Review Board Statement: Not applicable.

Informed Consent Statement: Not applicable.

Data Availability Statement: The data presented in this study are available in the article itself.

Acknowledgments: The authors wish to express their gratitude for the financial support that has made this study possible.

Conflicts of Interest: The authors declare no conflict of interest.

References

1. Franz, J.; Morse, S.; Pearce, J.M. Low-Cost Pole and Wire Photovoltaic Racking. *Energy Sustain. Dev.* **2022**, *68*, 501–511. [[CrossRef](#)]
2. Syafiq, A.; Balakrishnan, V.; Ali, M.S.; Dhoble, S.J.; Rahim, N.A.; Omar, A.; Bakar, A.H.A. Application of Transparent Self-Cleaning Coating for Photovoltaic Panel: A Review. *Curr. Opin. Chem. Eng.* **2022**, *36*, 100801. [[CrossRef](#)]
3. Liu, J.; Xie, X.; Li, L. Experimental Study on Mechanical Properties and Durability of Grafted Nano-SiO₂ Modified Rice Straw Fiber Reinforced Concrete. *Constr. Build. Mater.* **2022**, *347*, 128575. [[CrossRef](#)]
4. Rehman, M.S.U.; Umer, M.A.; Rashid, N.; Kim, I.; Han, J.-I. Sono-Assisted Sulfuric Acid Process for Economical Recovery of Fermentable Sugars and Mesoporous Pure Silica from Rice Straw. *Ind. Crops Prod.* **2013**, *49*, 705–711. [[CrossRef](#)]
5. Mehta, P.K. *Pozzolanic and Cementitious Byproducts as Mineral Admixtures for Concrete—A Critical Review*; ACI Special Publication 79; American Concrete Institute: Farmington Hills, MI, USA, 1983; 46p.
6. Roselló, J.; Soriano, L.; Santamarina, M.P.; Akasaki, J.L.; Monzó, J.; Payá, J. Rice Straw Ash: A Potential Pozzolanic Supplementary Material for Cementing Systems. *Ind. Crops Prod.* **2017**, *103*, 39–50. [[CrossRef](#)]
7. Thomas, B.S.; Yang, J.; Mo, K.H.; Abdalla, J.A.; Hawileh, R.A.; Ariyachandra, E. Biomass Ashes from Agricultural Wastes as Supplementary Cementitious Materials or Aggregate Replacement in Cement/Geopolymer Concrete: A Comprehensive Review. *J. Build. Eng.* **2021**, *40*, 102332. [[CrossRef](#)]
8. Abou-Sekkina, M.M.; Issa, R.M.; Bastawisy, A.E.-D.M.; El-Helece, W.A. Characterization and Evaluation of Thermodynamic Parameters for Egyptian Heap Fired Rice Straw Ash (RSA). *Int. J. Chem.* **2010**, *2*, 81. [[CrossRef](#)]
9. Munshi, S.; Sharma, R.P. Utilization of Rice Straw Ash as A Mineral Admixture in Construction Work. *Mater. Today Proc.* **2019**, *11*, 637–644. [[CrossRef](#)]
10. Pandey, A.; Kumar, B. Effects of Rice Straw Ash and Micro Silica on Mechanical Properties of Pavement Quality Concrete. *J. Build. Eng.* **2019**, *26*, 100889. [[CrossRef](#)]
11. Agwa, I.S.; Omar, O.M.; Tayeh, B.A.; Abdelsalam, B.A. Effects of Using Rice Straw and Cotton Stalk Ashes on the Properties of Lightweight Self-Compacting Concrete. *Constr. Build. Mater.* **2020**, *235*, 117541. [[CrossRef](#)]
12. Pandey, A.; Kumar, B. Evaluation of Water Absorption and Chloride Ion Penetration of Rice Straw Ash and Microsilica Admixed Pavement Quality Concrete. *Heliyon* **2019**, *5*, e02256. [[CrossRef](#)] [[PubMed](#)]
13. Pandey, A.; Kumar, B. Investigation on the Effects of Acidic Environment and Accelerated Carbonation on Concrete Admixed with Rice Straw Ash and Microsilica. *J. Build. Eng.* **2020**, *29*, 101125. [[CrossRef](#)]
14. Bories, C.; Borredon, M.-E.; Vedrenne, E.; Vilarem, G. Development of Eco-Friendly Porous Fired Clay Bricks Using Pore-Forming Agents: A Review. *J. Environ. Manag.* **2014**, *143*, 186–196. [[CrossRef](#)]
15. Duppati, S.; Gopi, R. Strength and Durability Studies on Paver Blocks with Rice Straw Ash as Partial Replacement of Cement. *Mater. Today Proc.* **2022**, *52*, 710–715. [[CrossRef](#)]
16. Singh, S.; Maiti, S.; Bisht, R.S.; Balam, N.B.; Solanki, R.; Chourasia, A.; Panigrahi, S.K. Performance Behaviour of Agro-Waste Based Gypsum Hollow Blocks for Partition Walls. *Sci. Rep.* **2022**, *12*, 3204. [[CrossRef](#)]

17. Tachaudomdach, S.; Hempao, S. Investigation of Compression Strength and Heat Absorption of Native Rice Straw Bricks for Environmentally Friendly Construction. *Sustainability* **2022**, *14*, 12229. [[CrossRef](#)]
18. Rajput, A.; Gupta, S.; Bansal, A. A Review on Recent Eco-Friendly Strategies to Utilize Rice Straw in Construction Industry: Pathways from Bane to Boon. *Environ. Sci. Pollut. Res.* **2022**, *30*, 11272–11301. [[CrossRef](#)] [[PubMed](#)]
19. Ataie, F. Influence of Rice Straw Fibers on Concrete Strength and Drying Shrinkage. *Sustainability* **2018**, *10*, 2445. [[CrossRef](#)]
20. Nguyen, C.V.; Mangat, P.S. Properties of Rice Straw Reinforced Alkali Activated Cementitious Composites. *Constr. Build. Mater.* **2020**, *261*, 120536. [[CrossRef](#)]
21. Nazerian, M.; Sadeghiipanah, V. Cement-Bonded Particleboard with a Mixture of Wheat Straw and Poplar Wood. *J. For. Res.* **2013**, *24*, 381–390. [[CrossRef](#)]
22. Karade, S.R.; Irle, M.; Maher, K. Assessment of Wood-Cement Compatibility: A New Approach. *Holzforschung* **2003**, *57*, 672–680. [[CrossRef](#)]
23. Canovas, M.F.; Selva, N.H.; Kawiche, G.M. New economical solutions for improvement of durability of Portland cement mortars reinforced with sisal fibers. *Mater. Struct.* **1992**, *25*, 417–422. [[CrossRef](#)]
24. Ma, L.F.; Kuroki, Y.; Eusebio, D.A.; Nagadomi, W.; Kawai, S.; Sasaki, H. Manufacture of bamboo cement composites. 1. Hydration characteristics of bamboo-cement mixtures. *Mokuzai Gakkaishi* **1996**, *42*, 34–42.
25. Sorrel, S. On a new magnesium cement. *C. R. Acad. Sci.* **1867**, *65*, 102–104.
26. Zhou, X.; Li, Z. Light-Weight Wood–Magnesium Oxychloride Cement Composite Building Products Made by Extrusion. *Constr. Build. Mater.* **2012**, *27*, 382–389. [[CrossRef](#)]
27. Sglavo, V.M.; De Genua, F.; Conci, A.; Ceccato, R.; Cavallini, R. Influence of Curing Temperature on the Evolution of Magnesium Oxychloride Cement. *J. Mater. Sci.* **2011**, *46*, 6726–6733. [[CrossRef](#)]
28. Chau, C.K.; Chan, J.; Li, Z. Influences of Fly Ash on Magnesium Oxychloride Mortar. *Cem. Concr. Compos.* **2009**, *31*, 250–254. [[CrossRef](#)]
29. Deng, D. The Mechanism for Soluble Phosphates to Improve the Water Resistance of Magnesium Oxychloride Cement. *Cem. Concr. Res.* **2003**, *33*, 1311–1317. [[CrossRef](#)]
30. Xiao, J.; Zuo, Y.; Li, P.; Wang, J.; Wu, Y. Preparation and Characterization of Straw/Magnesium Cement Composites with High-Strength and Fire-Retardant. *J. Adhes. Sci. Technol.* **2018**, *32*, 1437–1451. [[CrossRef](#)]
31. Li, Y.; Yu, H.; Zheng, L.; Wen, J.; Wu, C.; Tan, Y. Compressive Strength of Fly Ash Magnesium Oxychloride Cement Containing Granite Wastes. *Constr. Build. Mater.* **2013**, *38*, 1–7. [[CrossRef](#)]
32. Wang, J.; Zuo, Y.; Xiao, J.; Li, P.; Wu, Y. Construction of Compatible Interface of Straw/Magnesia Lightweight Materials by Alkali Treatment. *Constr. Build. Mater.* **2019**, *228*, 116712. [[CrossRef](#)]
33. Dao, T.N.; van de Lindt, J.W. Seismic Performance of an Innovative Light-Gauge Cold-Formed Steel Mid-Rise Building. In Proceedings of the Structures Congress 2012, Chicago, IL, USA, 29–31 March 2012; American Society of Civil Engineers: Reston, VA, USA, 2012.
34. Li, Z.; Guan, K. Research on Housing Industrialization and Necessity of Its Development. *J. Harbin Univ. Civ. Eng. Archit.* **1999**, *98*–102.
35. Girard, J.; Tarpay, T. Shear Resistance of Steel-Stud Wall Panels Shear Resistance of Steel-Stud Wall Panels. In Proceedings of the 6th International Specialty Conference on Cold-Formed Steel Structures, St. Louis, MO, USA, 16–17 November 2020.
36. He, B.-K.; Guo, P.; Wang, Y.-M. Experimental investigation on high strength cold-formed steel framing wall studs under axial compression loading. *J. Xi'an Univ. Archit. Technol.* **2008**, *40*, 567–573+579.
37. Bian, J.; Cao, W.; Xiong, C. Experiment on the compression performance of composite wall of cold-formed steel and tailing microcrystalline foam glass slab. *J. Harbin Inst. Technol.* **2019**, *51*, 86–93.
38. Qian, Z.; Pan, J.; Zhang, L. Research on Flexural Behavior of Light-Gauge Steel Stud Concrete Composite Wall Panels. *Ind. Constr.* **2020**, *50*, 32–37+4.
39. Wu, J.; Wang, Q.; Li, B. A study on compressive properties of cold-formed thin-walled steel frame fly ash ceramsite concrete wallboard. *New Build. Mater.* **2018**, *45*, 97–100. [[CrossRef](#)]
40. Lu, M.J. Thermal Optimization Strategy of External Wall in Low-Rise Light Steel Keel Structure Based on the Theory of Thermal Bridge. *AMR* **2013**, *671–674*, 2150–2153. [[CrossRef](#)]
41. *GBT50081-2019*; Standard Test Method for Physical and Mechanical Properties Of Concrete. China Building Industry Press: Beijing, China, 2019.
42. Wang, S.; Zhang, D.; Liu, G.; Wang, W.; Hu, M. Application of Hot-Wire Method for Measuring Thermal Conductivity of Fine Ceramics. *Mater. Sci.* **2016**, *22*, 560–564. [[CrossRef](#)]
43. *GB50176-2016*; Code for Thermal Design of Civil Building. China Building Industry Press: Beijing, China, 2016.
44. Li, F.; Li, J.; Xiao, M.; Ren, M. Impact Resistance of Lightweight Steel-Framed Foamed Concrete Composite Wall Panels. *Bull. Chin. Ceram. Soc.* **2022**, *41*, 68–75.

Disclaimer/Publisher's Note: The statements, opinions and data contained in all publications are solely those of the individual author(s) and contributor(s) and not of MDPI and/or the editor(s). MDPI and/or the editor(s) disclaim responsibility for any injury to people or property resulting from any ideas, methods, instructions or products referred to in the content.